Solar Energy Materials & Solar Cells 263 (2023) 112592

Contents lists available at ScienceDirect

Solar Energy Materials and Solar Cells

journal homepage: www.elsevier.com/locate/solmat

Evaluation of low-emissivity coatings with single, double, and triple silver layers

Natalia Herguedas, Enrique Carretero *

Departamento de Física Aplicada, Universidad de Zaragoza, C/Pedro Cerbuna, 12, 50009, Zaragoza, Spain

ARTICLE INFO

Keywords:
Low-emissivity coating
Thin film
Silver film
Sputtering
Optical properties
Transparent conducting film

ABSTRACT

In this work, a detailed study is conducted on the visible transmittance, solar reflectance, and emissivity properties of low-emissivity coatings composed of one, two, and three layers of silver. The results demonstrate significant enhancements in both optical and thermal properties achievable by increasing the number of silver layers, leading to coatings that are more transparent in the visible spectrum, more reflective in the near-infrared, with lower emissivity and lower sheet resistance. The aesthetic adjustment possibilities of the different structures are also examined, with coatings composed of three layers of silver being more flexible.

1. Introduction

The utilization of energy and its efficient management are gaining significant importance. One way to enhance building efficiency is through the application of low-emissivity coatings on their glass surfaces [1,2]. These coatings should allow visible sunlight to pass through, enabling natural illumination inside the building, while reflecting the infrared portion of the solar spectrum. Additionally, they must exhibit high reflectance in the thermal infrared region. Fig. 1a presents the solar spectrum alongside the ideal transmittance curves of low-emissivity coatings for both warm and cold climates. In cold climates, there is a desire for high transmittance of infrared solar radiation to heat the interior of the building [3]. The figure also illustrates the blackbody emission at room temperature, demonstrating that nearly all thermal radiation concentrates within wavelengths ranging from 3 to 50 μm. In Fig. 1b, the transmittance spectrum of a window glass is shown, revealing a high transmittance up to a wavelength of 3 μm, while for longer wavelengths, the glass becomes opaque. Additionally, the reflectance coefficient of the glass is also shown, indicating consistently low values across the entire range. These properties lead to significant energy losses in the glass due to the absorption and emission of thermal radiation. Finally, the reflectance spectrum of a glass with a low-emissivity coating is presented, showing a remarkable increase in reflectance, approaching unity.

One of the main methods for applying low-emissivity coatings is by depositing layers of noble metals onto the glass, such as Au, Ag, and Cu [4–7]. These metals possess high reflectance in the thermal infrared region. Furthermore, combining these metals with Transparent Layers (TL) allows for the adjustment of transmittance and reflectance spectra, especially in the visible region. Thus, by selecting the appropriate multilayer configuration, visible spectrum transmittance can be maximised while maximising infrared reflectance. Among the noble metals, silver (Ag) exhibits the most suitable optical properties for low-emissivity coatings [8]. It has been extensively studied and is widely used in the glass industry.

In the past, low-emissivity coatings have been developed using various transparent oxide materials such as SnO_2 [9,10], ZnO [5,11], AZO [12,13], TiO_2 [14], among others [15]. In this study, Aluminium-doped zinc oxide (AZO) has been utilized due to its favorable wetting properties for silver, leading to superior outcomes compared to other TL.

The basic structure of a low-emissivity coating is Substrate/TL (30–60 nm)/Ag (10–30 nm)/TL (30–70 nm), Fig. 2a. In other words, it consists of a layer of silver (Simple silver, SAG) sandwiched between TL layers with carefully adjusted thicknesses to enhance optical properties [16–18]. The first TL layer also improves adhesion and wetting of the silver, while the outer TL layer acts as a protective barrier against exposure to the atmosphere, thus improving the coating's durability [19–21].

Moreover, it is common to deposit a thin barrier layer of a metal like Ti, NiCr, to prevent silver oxidation during the deposition process [3, 22]. However, in the current study, the application of such a barrier

* Corresponding author.
E-mail address: ecarre@unizar.es (E. Carretero).

https://doi.org/10.1016/j.solmat.2023.112592
Received 30 July 2023; Received in revised form 21 September 2023; Accepted 5 October 2023
Available online 11 October 2023

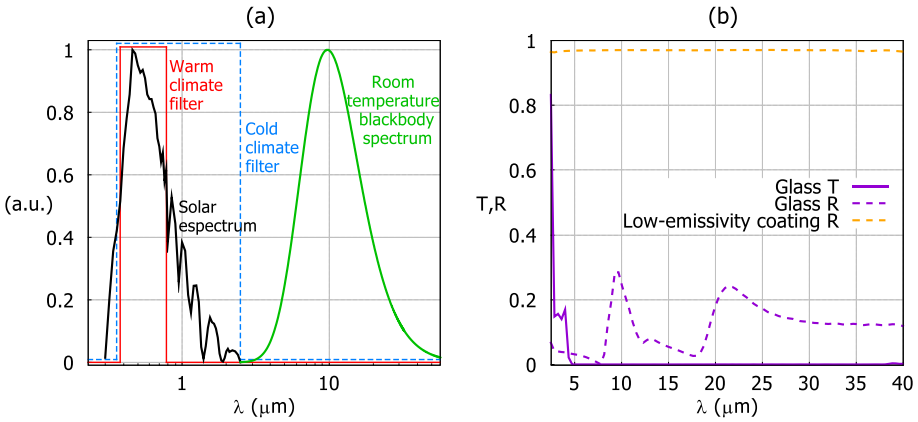

Fig. 1. (a) Solar and room temperature blackbody spectra along with ideal transmittance spectra for the coatings in warm and cold climates. (b) Transmittance and reflectance for the glasses that are used in this study, together with the reflectance of a low-emissivity coating.

layer was not deemed necessary as a ceramic AZO target was used, and only argon gas was utilized during the deposition process. This type of structure has also been employed in the production of transparent and conductive layers with low sheet resistance [23,24].

One way to enhance the photoenergetic properties of low-emissivity coatings is by depositing a multilayer composed of two silver layers (Double silver, DAG), with a structure of Substrate/TL/Ag/TL/Ag/TL [2,8,25], Fig. 2b. In this case, higher visible transmittance and infrared reflectance can be achieved, resulting in improved photoenergetic properties of the coating. Low-emissivity coatings with DAG enable a higher degree of customization for transmittance and reflectance spectra. The effect of the double silver layer can be likened to a Fabry-Perot interferometer, allowing us to adjust the wavelength of high transmittance [26].

To achieve improved properties, the deposition of coatings with a triple layer of silver (TAG) can be considered, with a structure like Substrate/TL/Ag/TL/Ag/TL/Ag/TL [27,28], Fig. 2c. These types of structures are suggested by various low-emissivity glass manufacturers [29,30], yet there is scarce scientific literature available concerning these specific configurations.

Another crucial aspect concerning low-emissivity coatings is their aesthetic appearance, given that these glazings are prominently featured on building facades [31].

This study presents a detailed analysis comparing the properties of low-emissivity coatings composed of multilayers with single, double, or triple layers of silver. An assessment of their photoenergetic properties is conducted based on the total thickness of the deposited silver, and finally, the potential for adjusting the aesthetic appearance of the coatings is explored. The coatings were deposited using an in-line sputtering deposition system with a geometry similar to that of industrial deposition systems (Fig. S1 in supplementary material).

2. Experimental setup

In this study, thin films were produced using a prototype industrial magnetron sputtering setup. The minimum pressure that can be obtained in the process chamber is on the order of 10^{-7} mbar. This installation features eight distinct magnetrons, four on each side, granting the ability to deposit up to four different materials onto samples. Each target used has dimensions of 600 × 100 mm. In this study we use silver and AZO. Silver has a purity of 99.99 %. AZO is a compound formed by doping Zinc Oxide (ZnO) with Aluminium Oxide (Al_2O_3) at a concentration of 2 % by weight and with 99.95 % of purity.

Two power supplies with a capacity of 10 kW were available. 2 kW and 500 W were used for AZO and silver deposition, respectively. Precise control of gas flows was achieved with mass flow controllers (MFCs). In this study, both AZO and silver were deposited using 300 sccm of argon

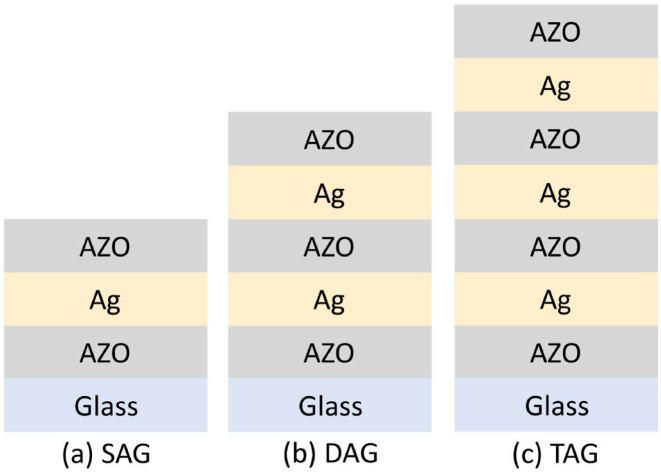

Fig. 2. Multilayer structure of (a) single, (b) double, and (c) triple silver layers.

for non-reactive sputtering deposition, which corresponds to a pressure of approximately $2{\cdot}10^{-7}$ mbar in the chamber.

A 5 × 5 cm low-iron sodium-calcium glass (Pilkington Optiwhite™) with a thickness of 4 mm was used as substate. Substrates were firstly cleaned with a special glass detergent (ACEDET 5509). To further enhance the adhesion of the layers and ensure optimal performance and quality of the thin films, an ion gun was employed in the sputtering chamber. For that specific purpose, a voltage of 2 kV and an argon flow rate of 50 sccm were employed.

The substrate holder of the installation was engineered to move linearly at a consistent velocity, guaranteeing uniform exposure for each point at the same height during the deposition process. Additionally, due to the magnetrons' larger dimensions compared to the samples, points along the same vertical line received equal exposure as well.

Under constant power and argon flow conditions, the thickness of the deposition is inversely proportional to the speed of the carrier. In order to calibrate this relationship, a monolayer of the material was deposited and then its thickness was measured with a profilometer, (DektakXT® model), which has a precision on the order of nanometres.

In order to identify the crystalline structure of materials, X-ray diffraction measurements are conducted at room temperature using a Ru2500 RIGAKU diffractometer, which has a rotative Cu anode, operated at 40 kV and 80 mA. A graphite monochromator is used to select K_α radiation ($\lambda = 0.15406$ nm). The diffraction angle, 2θ, ranges from 20° to 80° with a 0.03° step and t = 3s/step. The peaks that are obtained with this analysis allow for the calculation of the crystalline sizes, *D*, using the Debye-Sherrer equation:

$$D = \frac{K\,\lambda}{\beta \cos\theta}, \tag{1}$$

where K is the Scherrer constant (0.90), λ is the X-ray wavelength (0.15406 nm in this case), β is the full width at half maximum (FWHM) of the peak, and θ is the Bragg diffraction angle.

A morphology analysis is done with the Field Emission Scanning Electron Microscope (FESEM) Carl Zeiss MERLIN™. This FESEM equipment facilitates high-resolution observations down to 0.8 nm and accommodates a wide range of acceleration voltages, from 0.02 to 30 kV.

In order to conduct a compositional analysis of the samples, a time-of-flight secondary ion mass spectrometry (TOF-SIMS) is carried out using the TOF-SIMS 4 from ION-TOF GmbH. Bi^{3+} is used as a primary ion at 25 kV and 0.15 pA with an analysis area of 300 × 300 μm^2 and a cycle time of 100 μs. Cesium dual beam sputter gun is set to 2 keV energy.

Transmittance and reflectance spectra in UV–Vis/NIR were measured with a spectrophotometer which was developed by the Photonic Technologies Group from University of Zaragoza. It is capable of measuring wavelengths in a range of 300–2500 nm with an interval of 10 nm and the measurements are taken with an angle of incidence of 8°.

Transmittance spectra, $T(\lambda)$, from that spectrophotometer were used to calculate T_{VIS} and T_{SOLAR}, two of the photoenergetic factors that characterize low-emissivity and solar control coatings:

$$T_{VIS} = \frac{\int_{-\infty}^{\infty} T(\lambda) D_{65}(\lambda) V(\lambda) d\lambda}{\int_{-\infty}^{\infty} D_{65}(\lambda) V(\lambda) d\lambda}, \tag{2}$$

$$T_{SOLAR} = \frac{\int_{-\infty}^{\infty} T(\lambda) S(\lambda) d\lambda}{\int_{-\infty}^{\infty} S(\lambda) d\lambda}, \tag{3}$$

where $D_{65}(\lambda)$ is the standard illuminator defined by CIE, $V(\lambda)$ is the normalized human eye spectral sensitivity curve and $S(\lambda)$ is the solar spectrum. The wavelengths that we use in this study are the ones that the EN 410:2011 standard specifies [32].

A FTIR spectrophotometer with resolution of 16 cm^{-1} is used to measure reflectance spectra from 5000 to 200 cm^{-1} (2–50 μm). From this data the emissivity of the sample can be determined as

$$\varepsilon = 1 - R_{IR}, \tag{4}$$

where R_{IR} is calculated as an average of the reflectance in 30 wavelengths, as indicated in the EN 12898:2019 standard [33].

Sheet resistance was determined using a 4-point probing method with a Jandel RM3000 instrument, which can measure from 1 mΩ/□ to 100 MΩ/□. Sheet resistance, $R_{\square}$, is a very commonly used parameter in the field because it has a relationship to emissivity, given by Ref. [34]:

$$\varepsilon = 0.0106 \cdot R_{\square}, \tag{5}$$

which is an approximation for metallic or semiconductor coatings that have a low sheet resistance ($R_{\square} \ll z_0$, where $z_0 = 377\ \Omega$ is the impedance of vacuum) in the wavelength range $\lambda > 3$ μm.

In the study, a thermal camera was utilized to observe the variations in emissivity among different samples. The thermal camera, with a specific emissivity value set at 1 for this study, determines the apparent temperature of objects based on the radiation it receives. The camera receives less radiation from the samples with lower emissivity, resulting in a lower apparent temperature assignment. The FLIR AX8 camera was used in the study and it has a thermal sensitivity of 0.1 °C at 30 °C.

3. Results

3.1. Structural and TOF-SIMS analysis

First of all, we show the results of X-ray diffraction of a monolayer of 100 nm of AZO in order to analyse the structure of AZO transparent layers. The black line of Fig. 3 shows that we obtain a peak in 34.10°, corresponding to the (002) plane of ZnO. This is consistent with [35–38], in which (002) plane is obtained preferentially when depositing AZO through sputtering even if pressure, temperature or power are modified. In other studies [39], it has been observed that the growth orientation shifts between (002) and (103) with an increase in sputtering power. Other planes such as (100), (101) and (110) are obtained in Ref. [40] with a change of the annealing temperature.

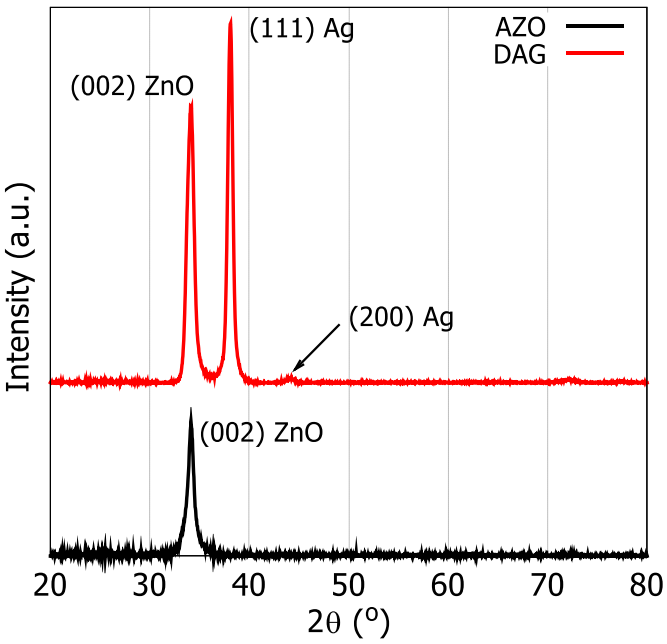

Fig. 3. X-ray diffraction results for a monolayer of AZO and a double silver layer of 50 nm total silver thickness.

Table 1
Results for the peaks of the X-ray diffraction measurements.

	2θ (°)	FWHM (°)	D (nm)
AZO	34.10	0.86	9.71
Ag	38.09	0.63	13.44

X-day diffraction measurements are also conducted in a DAG sample which has a total of 50 nm of silver. The result of the analysis is the red line of Fig. 3, in which there are three peaks. The first one corresponds to plane (002) of ZnO and the next two correspond to planes (111) and (200) of Ag. This is also consistent with other works, such as [41].

Adjusting the first two peaks to a Gaussian shape, we obtain the centre and the FWHM, with which we can obtain the crystalline sizes. In Table 1 we show the results.

Following the analysis with X-ray diffraction, Fig. S2 of the supplementary material shows FESEM images of a 60 nm TAG.

Finally, we present the TOF-SIMS measurements of the 50 nm double silver sample, which has also been analysed with X-ray diffraction (Fig. 4a), and the 60 nm triple silver sample, which has undergone FESEM analysis (Fig. 4b). The blue line represents the respective two and three silver layers, while the AZO layers are indicated by the ZnO^- red line and the Al^- green line. The orange line indicates that the substrate has Si^-. The thicknesses of the layers are coherent with those presented in Tables S4 and S5 of the supplementary material.

In Figs. S3 and S4 of the supplementary material we present the 3D cross sections map of ZnO^-, Ag^-, Si^- and Al^- of the samples and in Fig. 5 we overlay the maps of the TAG sample in order to better visualise the layer structure of the samples.

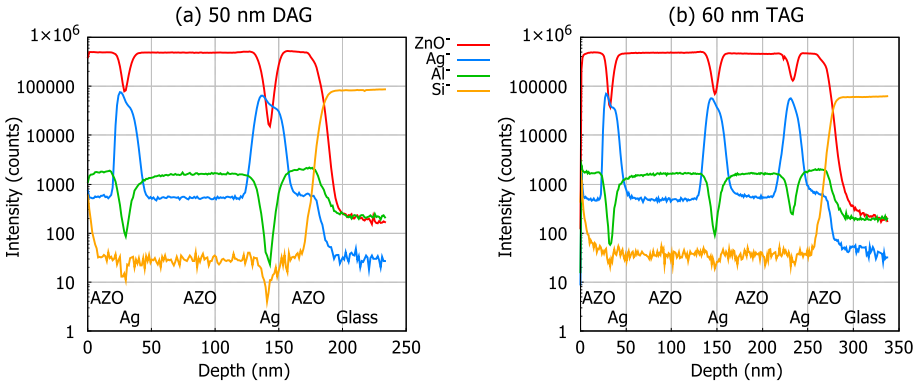

Fig. 4. Compositional analysis through TOF SIMS as a function of depth for (a) a 50 nm DAG sample and (b) a 60 nm TAG sample.

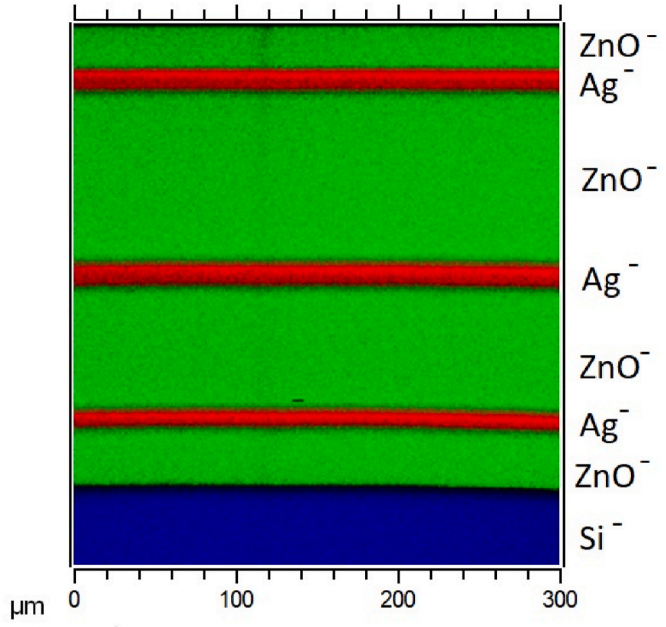

Fig. 5. Overlay of the 3D cross sections of ZnO^{-}, Ag^{-} and Si^{-} of a 60 nm TAG sample.

3.2. Comparison of T_{VIS} and ε balance

In Fig. 6, we present the transmittance spectra of single, double, and triple silver layers with the same total silver thickness (40 nm) and AZO thicknesses that maximise the T_{VIS} factor. This criterion for the AZO thicknesses will be used in all the samples that are presented in this subsection. When additional silver layers are added, the observed effect

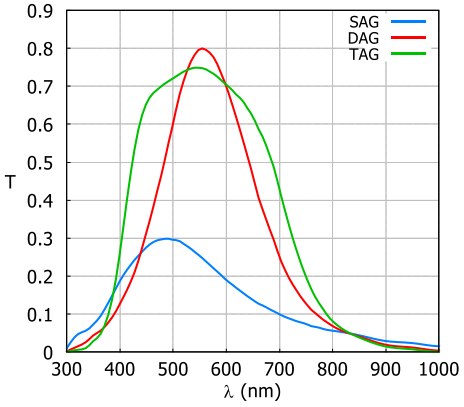

Fig. 6. Transmittance spectra for single, double and triple silver layers with the same silver thickness (40 nm) and AZO thicknesses that maximise the T_{VIS} factor.

is a sharper rise and fall of the transmittance spectrum peak in the visible region. Moreover, the upper part of the peak exhibits a more rectangular appearance, approaching closer to the ideal case. It is important to clarify that it may seem that the structure with three layers of silver has a lower peak than the structure with two layers, but T_{VIS} is higher for the three layers structure because the peak is wider.

If we study the evolution of these spectra with the quantity of silver, Fig. 7, the same tendency can be observed for each structure: the more the total thickness of the silver, the narrower the peak in the transmittance spectrum and the lower of the maximum transmittance in the peak (the thicknesses of the layers comprising the low-emissivity coatings are presented in Tables S1–S5 in the supplementary material). This implies that T_{VIS} and T_{SOLAR} are lower. However, this effect is much more noticeable in the case of single silver layers. In double silver structures, the width of the peak narrows considerably, but the decrease in the

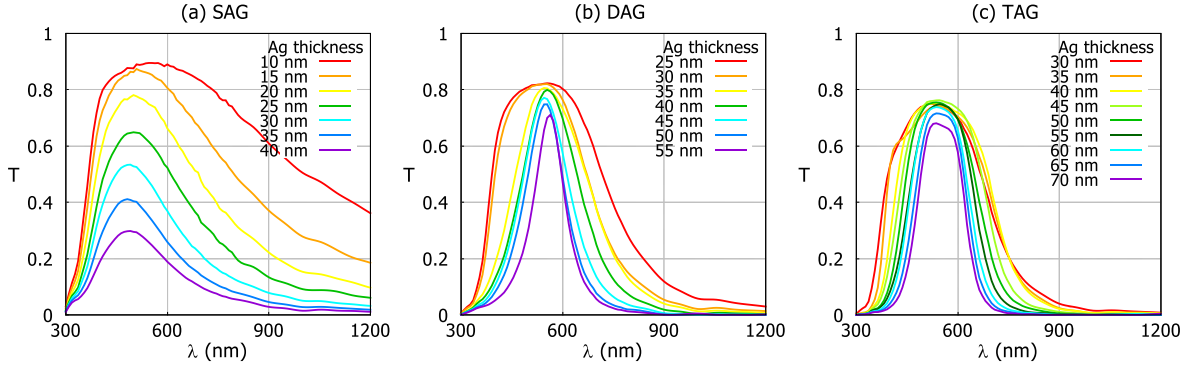

Fig. 7. Evolution of transmittance spectra for single (a), double (b) and triple (c) silver layers with the total tickness of silver.

transmittance of the centre of the peak is not as accentuated as in the single silver structure. Moreover, regarding triple silver structure, the width of the peak does not decrease so much as in double silver layers.

Both T_{VIS} and T_{SOLAR} decrease with the increasing amount of silver. However, it is desirable for T_{VIS} to be as high as possible, while T_{SOLAR} should be relatively lower. It is important to consider that the visible range is also a factor in the T_{SOLAR} calculation, making it impossible for T_{SOLAR} to be zero. To assess this balance, we calculate the T_{VIS}/T_{SOLAR} ratio, which should ideally be high, indicating that a significant portion of the solar radiation passing through the sample is visible light. This ratio is presented in Fig. 8 for single, double and triple silver layers.

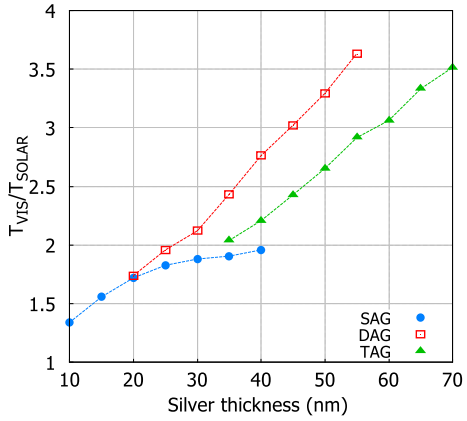

Fig. 8. T_{VIS}/T_{SOLAR} ratio as a function of the total silver thickness for single, double and triple silver layers.

Single silver layers have a very low ratio compared to double and triple layers, as they allow minimal transmission of both solar radiation and visible light. In the case of double and triple silver layers, double silver layers demonstrate a higher ratio for each silver thickness, making them superior in that aspect. However, it must be emphasised that this is a result of the transmittance peak being very narrow (Fig. 6), this is undesirable because it has a colour with a very high chromatic component, which will be further explained in subsection 3.2.

Regarding reflection, spectra are closer to 1 when the thickness of silver is greater, which implies that emissivity will be lower with the total amount of silver. VIS-NIR spectra are shown in Fig. 9, and thermal infrared spectra are included in Fig. S5 of the supplementary material.

The objective of low-emissivity structures for solar control is that the transmittance peak is as rectangular and as high as possible. Therefore, the more the total tickness of silver, the worse for the transmittance spectrum in the visible region. Nevertheless, the reflectance should be as close to 1 as possible in infrared, so the more the tickness of silver, the better.

To do a further study of this relationship, in Fig. 10 we represent T_{VIS} on one axis and emissivity on the other axis (emissivity has been calculated based on the measurements of thermal infrared reflectance). For double and single silver layers, the thicker the silver layers, the less the T_{VIS} factor and the less emissive the samples are. Regarding single and double silver structures, we can see that for the same thickness of silver, single silver layers have lower emissivity than double silver layers. Nevertheless, double silver layers with higher amount of silver get the same emissivity with higher T_{VIS}, so the balance is better. Taking into account triple silver layers, the balance does not enhance as clearly as before: if triple silver layer have less than 55 nm (a value of emissivity higher than 0.018), double silver layers get the same emissivity with

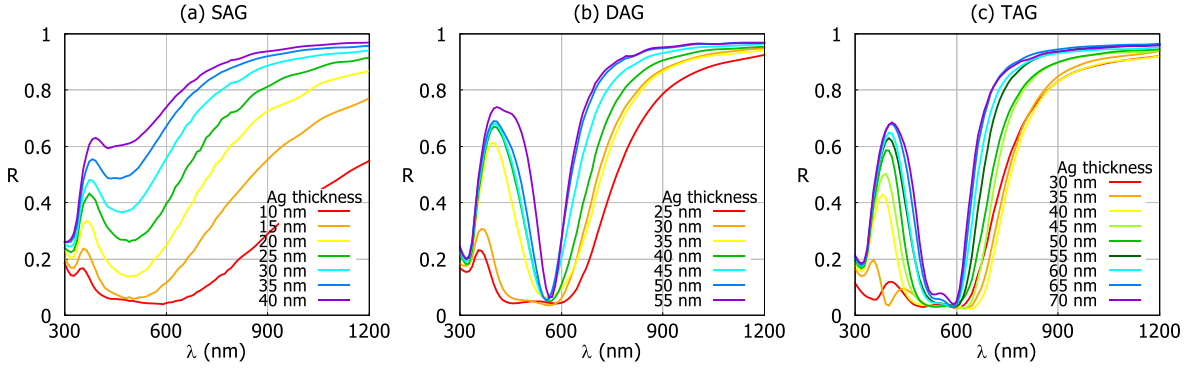

Fig. 9. Evolution of reflectance spectra on the coating side in VIS-NIR for single (a), double (b) and triple (c) silver layers with the total tickness of silver.

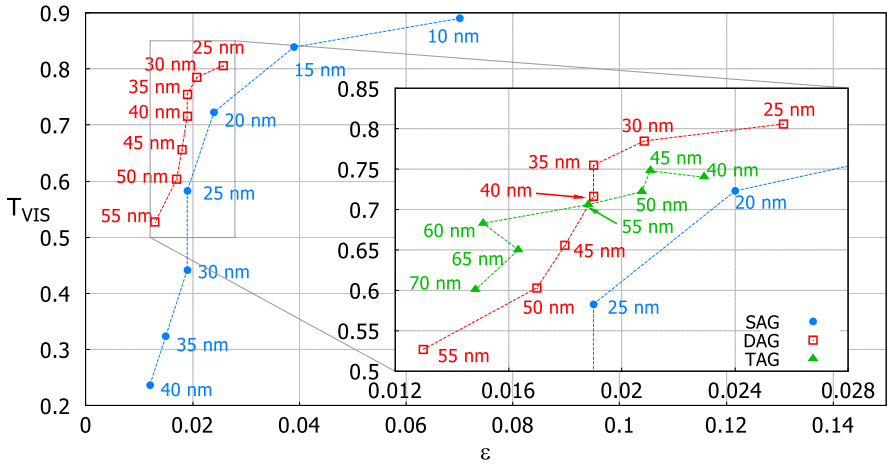

Fig. 10. T_{VIS} versus ε for the three types of structures with different total silver thicknesses.

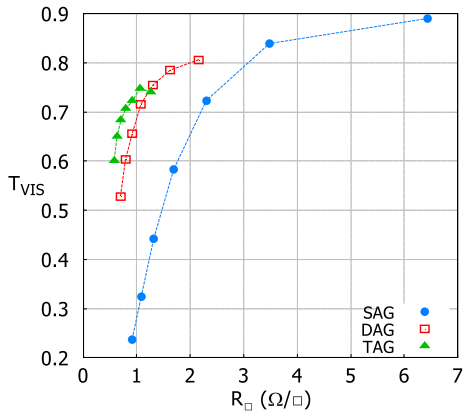

Fig. 11. T_{VIS} versus sheet resistance balance for the three types of structures.

better T_{VIS} and with less amount of silver; if triple silver layers have more that 55 nm, they do improve the balance.

The measurements of thermal infrared reflectance (and consequently, the emissivity) are highly noisy due to the lack of perfect uniformity in samples and the pattern, the drift of the spectrophotometer lamp power, and the presence of CO_2 and H_2O in the environment, among other factors. For this reason, we also measure sheet resistance, which is commonly studied in similar works due to its relationship to emissivity. In Fig. 11, we replot the graph from Fig. 10, replacing emissivity with sheet resistance. We can observe that the trend remains the same, but triple silver layers show an improvement compared to double silver structures at every point except for the first one. The measurements of sheet resistance are more accurate, but the relationship between emissivity and sheet resistance is obscured by the presence of layers that have infrared absorption bands. As a result, the fact that sheet resistance measurements exhibit a monotonic trend with the amount of silver does not necessarily imply the same trend for emissivity. This result shows that this type of multilayer structures with a triple layer of silver can also be used to obtain coatings that are more transparent and conductive. This could be applicable in other areas, for example, in the production of transparent electrical contacts.

Another way to compare the emissivity of different structures is by using a thermal camera. We placed a glass without any coating and glasses with single, double, and triple silver layer structures with the same total silver thickness on a heating plate at approximately 215 °C. The camera image is presented in Fig. 12. Firstly, the uncoated glass exhibits the highest temperature in the image, indicating that it emits the most. Additionally, the borders of the coated samples (without any coating) display the same colour, implying the same apparent temperature. Regarding the centers of the coatings, the structure with a single silver layer exhibits a lower apparent temperature than the one with two layers, and similarly, lower than the one with three layers. This implies that the single layer is the least emissive of the three. This observation aligns with the findings shown in Fig. 10.

Besides studying different structures, we take images of the same structure but with different silver thicknesses. Simple, double and triple silver layers structures are shown in Fig. 13. In all of them, apparent temperature decreases with increasing amount of silver in the sample. This suggests that the more silver thickness of the sample, the less emissive the sample is, just like in sheet resistance.

3.3. Chromatic behaviour of double and triple silver layers

It is not only important to study what happens when the AZO thicknesses maximise the T_{VIS} factor but also what happens when the thicknesses result in a specific colour for the sample.

As an example of chromatic objective, we aim for the samples to be neutral in colour. Ideally, they should be neutral in the colours of transmittance and reflectance on both sides. However, achieving this is challenging, even theoretically. Therefore, we decided to make them neutral in transmittance and reflectance on the glass side.

We use CIELab colour space to mathematically describe differences in colour due to its homogeneity. Let ΔE describe the difference between the chromatic coordinates, a* and b*, of certain colour and those of the neutral colour (a* = b* = 0):

$$\Delta E = \sqrt{a^{*2} + b^{*2}} \ . \tag{7}$$

The objective is to achieve $\Delta E < 3$ for neutral colours, as that is the sensitivity of the human eye.

An iterative adjustment process is carried out, in which the experimental samples are progressively fitted to the simulations that have been previously conducted and represent the objective. These simulations were performed to find the AZO thicknesses that maximise the T_{VIS} factor among those that achieve $\Delta E < 3$ for transmittance and reflectance on the glass side.

Table 2 displays the CIELab coordinates of the samples that maximise the T_{VIS} factor and those of the neutral samples for four values of silver thickness for the case of two silver layers. It is evident that the objective has been achieved, as the ΔE values in transmittance and glass reflectance are very low for neutral samples (let us remember that colour in coating reflection has not been optimised). For the case of 25 nm of silver, we observe a minimal difference between the colours of the sample that maximise T_{VIS} and the neutral one. This is due to the fact that the spectra are already very flat in the samples that maximise T_{VIS}, as shown in Fig. 14a. However, for larger silver thicknesses, such as 50 nm, there is a significant difference. This is because the spectra that maximise T_{VIS} have a very narrow peak, resulting in a colour with very

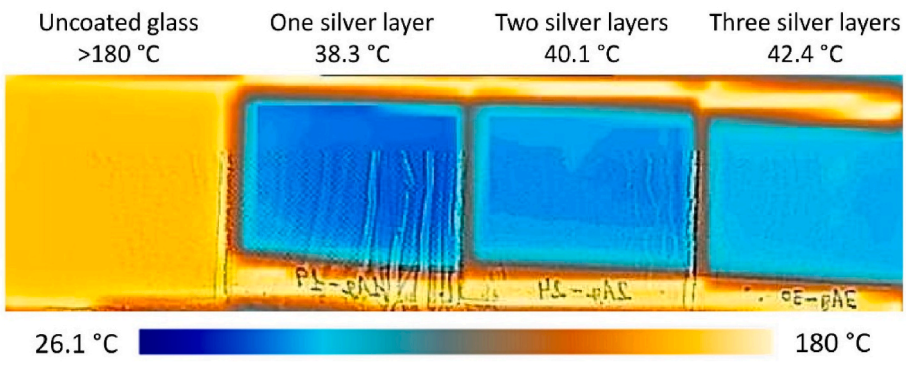

Fig. 12. Image from the thermal camera for uncoated glass, and single, double and triple layers with 30 nm of silver, when they are on a heating plate at around 215 °C.

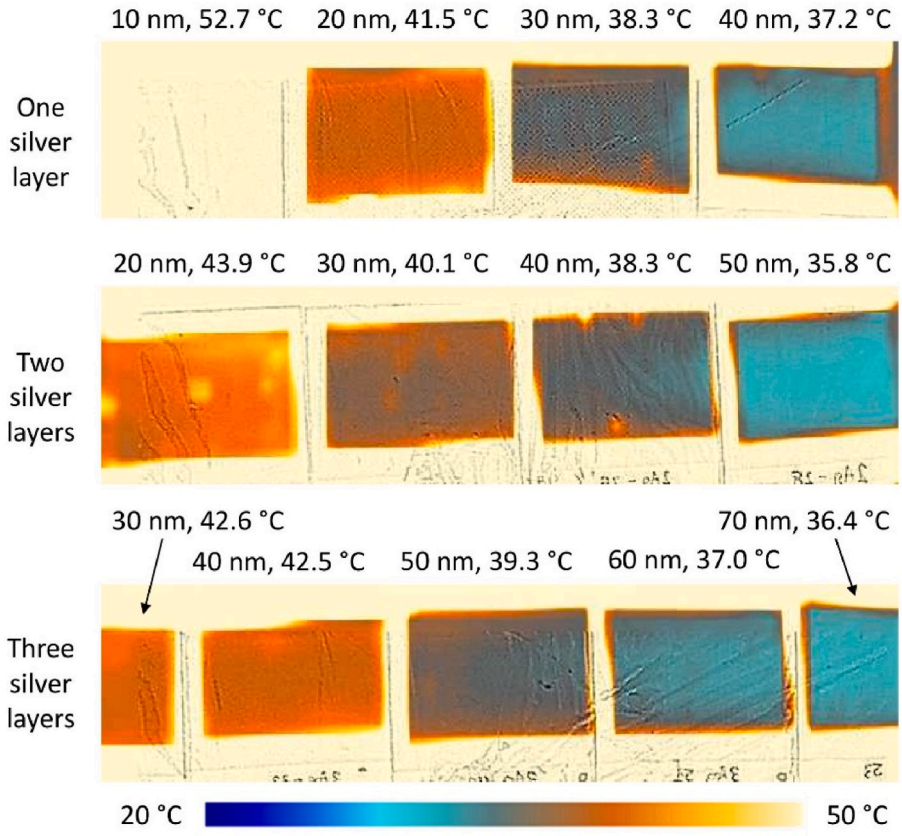

Fig. 13. Image from the thermal camera for several single, double and triple layers with different thicknesses of silver, when they are on a heating plate at around 215 °C.

Table 2
CIELab coordinates of the transmission and reflection in both sides' colours of the two silver layers samples of subsection 3.1 and the neutral ones.

		Samples with max T_{VIS}				Neutral samples			
Silver thickness (nm)		25	30	40	50	25	30	40	50
T	L*	91.9	91.0	87.0	81.1	88.8	81.2	68.8	57.8
	a*	−3.7	−7.8	−17.0	−30.4	−3.4	−1.6	−4.3	−8.0
	b*	3.2	4.0	36.6	40.0	−0.5	1.8	2.5	3.7
	ΔE	4.9	8.8	40.4	50.2	3.4	2.4	5.0	8.8
R_{glass}	L*	29.1	32.4	49.5	59.2	32.2	50.1	69.2	80.7
	a*	6.0	21.2	28.8	38.1	3.7	−5.9	0.4	2.8
	b*	−8.6	−11.0	−46.2	−37.8	2.8	−6.9	−2.1	1.5
	ΔE	10.5	23.9	54.4	53.7	4.6	9.1	2.1	3.2
$R_{coating}$	L*	26.6	28.6	45.8	54.4	28.3	49.6	39.3	67.6
	a*	4.6	20.5	28.4	38.0	−16.1	−35.7	−41.9	−39.8
	b*	0.6	−6.4	−54.3	−45.2	−0.3	−9.1	−15.9	−21.9
	ΔE	4.6	21.5	61.3	59.1	16.1	36.8	44.8	45.4

high chromatic coordinates. This is shown in Fig. 14b.

The same analysis can be done for triple silver layers, leading to the results of Table 3. There is a substantial improvement in the coordinates for neutral samples, even for the reflection on coating side, although those coordinates are not so low as transmission and glass reflection because they were not considered in the optimisation. Specially transmission has very low values of Δ*E*, even lower than 3. It is important to note that triple silver structures are more challenging to adjust experimentally because they have more layers to take into account.

Tables 2 and 3 demonstrate that it is possible to achieve samples that satisfy the chromatic objective with both double and triple silver layers. It is worth studying how the T_{VIS} factor and emissivity have changed to attain this goal.

In Fig. 15 the relative difference between the samples that maximise T_{VIS} and those that are neutral is illustrated. We consider the value for the samples that maximise T_{VIS} as the reference. We observe that for both double and triple silver layers, the relative difference increases with the thickness of silver. This is because the transmittance spectrum of the samples that maximise T_{VIS} and have lower silver thicknesses is quite flat, leading to a lesser difference with the spectrum of the neutral sample. Conversely, the transmittance spectrum of the samples that maximise T_{VIS} but have higher silver thicknesses exhibits a narrower peak. As a result, when adjusting it to be flatter in the visible region, T_{VIS} decreases more. This can be seen in Fig. 14. Although the tendency with the silver thickness is the same for double and triple silver layers, the relative difference is lower with triple silver layers.

In Fig. 16, a similar analysis is conducted, but for emissivity. Neither double nor triple silver layers exhibit a monotonous trend with the

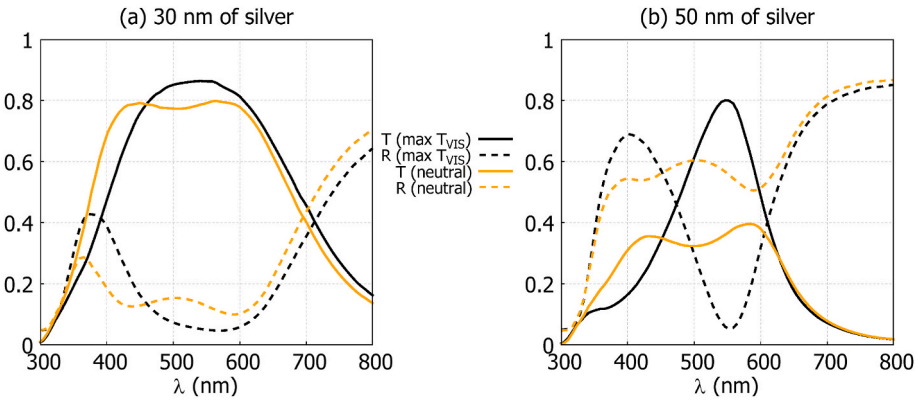

Fig. 14. Transmittance and glass reflectance spectra for DAG samples that maximise T_{VIS} factor and DAG neutral samples for (a) 30 nm of silver and (b) 50 nm of silver.

Table 3
CIELab coordinates of transmission and reflection in both sides' colours of the three silver layers samples of subsection 3.1 and the neutral ones.

		Samples with max T_{VIS}			Neutral samples		
Silver thickness (nm)		40	50	60	40	50	60
T	L*	88.8	87.8	85.7	78.7	72.9	68.3
	a*	−6.5	−14.8	−23.1	−4.1	−1.3	−1.1
	b*	7.3	17.8	29.5	1.6	1.9	2.8
	ΔE	9.8	23.1	37.5	4.4	2.3	3.0
R_{glass}	L*	28.3	33.0	38.7	37.5	56.8	65.8
	a*	16.7	39.3	50.2	1.1	−1.3	−0.7
	b*	−24.8	−40.7	−50.4	−5.6	10.0	14.0
	ΔE	29.9	56.6	71.1	5.7	10.1	14.0
$R_{coating}$	L*	22.4	27.2	34.4	54.4	63.3	68.0
	a*	15.9	43.5	50.2	−17.8	−24.6	−30.1
	b*	−27.0	−50.9	−59.1	−5.3	4.7	2.5
	ΔE	31.3	67.0	77.5	18.6	25.0	30.2

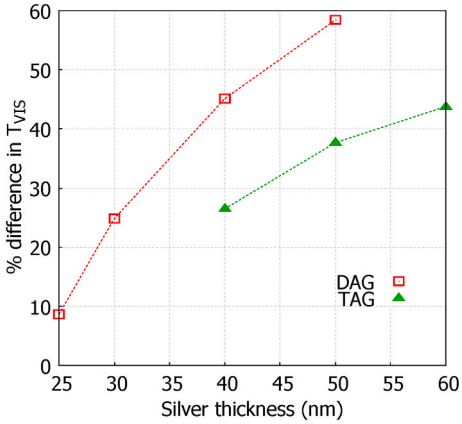

Fig. 15. Relative difference of T_{VIS} between samples that maximise T_{VIS} and neutral samples, taking as reference the samples that maximise T_{VIS}.

amount of silver, but the relative difference is lower for triple silver layers.

Therefore, the conclusion is that both double and triple silver layers can achieve a chromatic objective, but with triple silver layers there is less compromised in terms of T_{VIS} and emissivity.

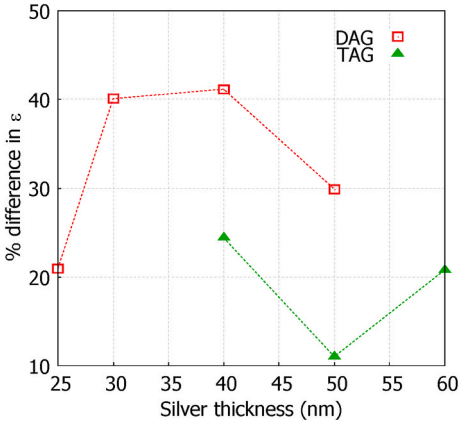

Fig. 16. Relative difference of ε between samples that maximise ε and neutral samples, taking as reference the samples that maximise T_{VIS}.

4. Conclusions

This study began by investigating the visible transmittance factor and emissivity in samples in which AZO thicknesses were chosen to maximise T_{VIS}. The results demonstrate that the same amount of silver in a single silver layer leads to a lower emissivity compared to a double silver layer, and similarly, to a triple silver layer. By conducting series of samples with different total silver thicknesses and studying their T_{VIS} and emissivity, the conclusion was that triple silver structures only provide an improvement if they have more than 55 nm of total silver thickness, resulting in an emissivity of 0.0188. For higher emissivity values, the better option is to use a double silver structure, which not only uses a lower silver thickness (reducing costs), but also achieves higher visible transmittances.

The sheet resistance measurements and the thermal camera readings make it evident that within each type of structure, as the amount of silver used increases, the resulting emissivity decreases. The triple silver layer structures could also be a good option for manufacturing transparent and conductive electrical contacts.

It has also been attempted to achieve a specific chromatic objective for the samples, which, as an example, has been chosen to be the neutral colour. Samples with neutral colours in transmission and reflection on the glass side have been designed for both two and three layers of silver. It has been found that it is possible to achieve such samples for both structures, but this comes with a decrease in visible transmission and an increase in emissivity compared to its optimum values. However, the worsening required for samples with three layers of silver is lower than that for two layers of silver, indicating that these structures do represent

an improvement in this aspect.

CRediT authorship contribution statement

Natalia Herguedas: Writing – review & editing, Writing – original draft, Software, Methodology, Investigation, Formal analysis, Data curation, Conceptualization. **Enrique Carretero:** Writing – review & editing, Writing – original draft, Project administration, Funding acquisition, Conceptualization.

Declaration of competing interest

The authors declare the following financial interests/personal relationships which may be considered as potential competing interests:

Enrique Carretero reports financial support was provided by Gobierno de Aragón. Enrique Carretero reports financial support was provided by Spanish Ministerio de Ciencia e Innovación. Enrique Carretero reports financial support was provided by Cátedra Ariño Duglass - Unizar.

Data availability

Data will be made available on request.

Acknowledgements

We gratefully acknowledge financial support from the Spanish Ministerio de Ciencia e Innovación, under the project RTC2019-007368-3, the Catedra Ariño Duglass and the "Departamento de Ciencia, Universidad y Sociedad del Conocimiento del Gobierno de Aragón" (group T20_20R). Authors would like to acknowledge the use of Servicio General de Apoyo a la Investigación-SAI, Universidad de Zaragoza. We also thank the Nanotechnology and Surface Analysis Service of the CACTI-University of Vigo for performing the TOF-SIMS analysis.

Appendix A. Supplementary data

Supplementary data to this article can be found online at https://doi.org/10.1016/j.solmat.2023.112592.

References

[1] B.P. Jelle, S.E. Kalnaes, T. Gao, Low-emissivity materials for building applications: a state-of-the-art review and future research perspectives, Energy Build. 96 (2015) 329–356, https://doi.org/10.1016/j.enbuild.2015.03.024.
[2] C. Schaefer, G. Bräuer, J. Szczyrbowski, Low emissivity coatings on architectural glass, Surf. Coating. Technol. 93 (1997) 37–45, https://doi.org/10.1016/S0257-8972(97)00034-0.
[3] G. Ding, C. Clavero, Silver-Based Low-Emissivity Coating Technology for Energy-Saving Window Applications, IntechOpen, 2017, https://doi.org/10.5772/67085.
[4] G.K. Dalapati, A.K. Kushwaha, M. Sharma, V. Suresh, S. Shannigrahi, S. Zhuk, S. Masudy-Panah, Transparent heat regulating (THR) materials and coatings for energy saving window applications: impact of materials design, micro-structural, and interface quality on the THR performance, Prog. Mater. Sci. 95 (2018) 42–131, https://doi.org/10.1016/j.pmatsci.2018.02.007.
[5] M. Rabizadeh, M.H. Ehsani, M.M. Shahidi, ZnO/metal/ZnO (metal = Ag, Pt, Au) films for energy-saving in windows application, Sci. Rep. 12 (2022), 15575, https://doi.org/10.1038/s41598-022-20043-8.
[6] K. Sun, D. Zhang, H. Yin, L. Cheng, H. Yuan, C. Yang, Preparation of AZO/Cu/AZO films with low infrared emissivity, high conductivity and high transmittance by adjusting the AZO layer, Appl. Surf. Sci. 578 (2022), 152051, https://doi.org/10.1016/j.apsusc.2021.152051.
[7] D. Zhang, K. Sun, H. Yin, L. Cheng, H. Yuan, C. Yang, Optimization of photoelectric properties and temporal stability of AZO/Ti/Cu/AZO films by insertion of Ti layer for low emissivity applications, Mater. Sci. Eng., B 293 (2023), 116471, https://doi.org/10.1016/j.mseb.2023.116471.
[8] J.-H. Lee, S.-H. Lee, K.-L. Yoo, N.-Y. Kim, C.K. Hwangbo, Deposition of multi-period low-emissivity filters for display application by RF magnetron sputtering, Surf. Coating. Technol. (2002) 477–481, https://doi.org/10.1016/S0257-8972(02)00293-1, 158–159.
[9] S.J.M. Baygi, Effect of the thin silver layer in SnO2/Ag/SnO2 nano-coatings with low emission for energy storage, J. Electron. Mater. 52 (2023) 4532–4539, https://doi.org/10.1007/s11664-023-10339-4.
[10] E. Carretero, A. Cueva, J. Preciado-Garbayo, P. Sevillano, Improved photoenergy properties of low-emissivity coatings deposited by sputtering with an ion gun treatment, Vacuum 205 (2022), 111485, https://doi.org/10.1016/j.vacuum.2022.111485.
[11] S. Chaudhuri, D. Bhattacharyya, A.B. Maity, A.K. Pal, Surface coatings for solar application, in: R.P. Agarwala (Ed.), SURFACE COATINGS FOR ADVANCED MATERIALS, Trans Tech Publications Ltd, Stafa-Zurich, 1997, pp. 181–206. https://doi.org/10.4028/www.scientific.net/MSF.246.181.
[12] L. Si-Ning, Z. Yan-Wen, S. Tian-Yi, W. Fa-Yu, Fabrication and characterization of the AZO/Ag/AZO transparent conductive films prepared by RF magnetron sputtering using powder targets, nanosci, Nanotechnol. Lett. 7 (2015) 743–748, https://doi.org/10.1166/nnl.2015.2027.
[13] D. Miao, S. Jiang, S. Shang, Z. Chen, Highly transparent and infrared reflective AZO/Ag/AZO multilayer film prepared on PET substrate by RF magnetron sputtering, Vacuum 106 (2014) 1–4, https://doi.org/10.1016/j.vacuum.2014.02.021.
[14] J. Kulczyk-Malecka, P.J. Kelly, G. West, G.C.B. Clarke, J.A. Ridealgh, K.P. Almtoft, A.L. Greer, Z.H. Barber, Investigation of silver diffusion in TiO2/Ag/TiO2 coatings, Acta Mater. 66 (2014) 396–404, https://doi.org/10.1016/j.actamat.2013.11.030.
[15] K. Mizukoshi, T. Yamamura, Y. Tomioka, M. Kawamura, Optimization of lowermost layer material for low-resistivity Ag-based multilayer structure in low-emissivity glass, Thin Solid Films 739 (2021), 138996, https://doi.org/10.1016/j.tsf.2021.138996.
[16] A. Thelen, Design of Optical Interference Coatings, McGraw-Hill, 1989.
[17] N. Kaiser, H.K. Pulker, Optical Interference Coatings, Springer, 2013.
[18] R.R. Willey, Practical Design of Optical Thin Films, fifth ed., Lulu.com, 2018.
[19] M.B. Cinali, O.D. Coskun, Optimization of physical properties of sputtered silver films by change of deposition power for low emissivity applications, J. Alloys Compd. 853 (2021), 157073, https://doi.org/10.1016/j.jallcom.2020.157073.
[20] F. Bocchese, I. Brown, D. Cornil, P. Moskovkin, J. Muller, S.D. Kenny, R. Smith, S. Lucas, Low-E glass improvement by the understanding and control of the Ag growth, Appl. Surf. Sci. 611 (2023), 155600, https://doi.org/10.1016/j.apsusc.2022.155600.
[21] A.R.C. Hernández, R.I.R. Ontiveros, H.E.E. Ponce, J.M.O. Ramírez, J.R.P. Michel, J. A.D. Moller, Effect of silver on structural, optical, and electrical properties of ZnO: Al/Ag/ZnO:Al thin films, Nova Scientia 14 (2022), https://doi.org/10.21640/ns.v14i29.3038.
[22] K. Mizukoshi, T. Yamamura, Y. Tomioka, M. Kawamura, Effect of blocking layer on achieving low sheet resistances in low-E multilayer structures, Jpn. J. Appl. Phys. 62 (2023), 045501, https://doi.org/10.35848/1347-4065/acc827.
[23] C. Guillén, J. Herrero, TCO/metal/TCO structures for energy and flexible electronics, Thin Solid Films 520 (2011) 1–17, https://doi.org/10.1016/j.tsf.2011.06.091.
[24] C. Zhang, C. Ji, Y.-B. Park, L.J. Guo, Thin-metal-Film-based transparent conductors: material preparation, optical design, and device applications, Adv. Opt. Mater. 9 (2021), 2001298, https://doi.org/10.1002/adom.202001298.
[25] J. Ebisawa, E. Ando, Solar control coating on glass, Curr. Opin. Solid State Mater. Sci. 3 (1998) 386–390, https://doi.org/10.1016/S1359-0286(98)80049-1.
[26] Q. Li, J. Gao, H. Yang, X. Wang, H. Liu, Z. Li, Mechanism investigation of a narrow-band super absorber using an asymmetric Fabry-Perot cavity, Opt. Quant. Electron. 49 (2017) 159, https://doi.org/10.1007/s11082-017-0998-3.
[27] T. Horiuchi, K. Yoshimura, Solar heat gain coefficient and heat transmission coefficient of Al-doped ZnO thin-film coated low-emissivity glass, J. Ceram. Soc. Japan. 128 (2020) 220–223, https://doi.org/10.2109/jcersj2.19217.
[28] J. Wu, X. Qian, C. Liu, Y. Ji, S. Yu, Design and realization of neutral-tinted low-E film, Vacuum 203 (2022), 111228, https://doi.org/10.1016/j.vacuum.2022.111228.
[29] G. Ding, B.W. Den, Y. Lu, C. Clavero, D. Schweigert, S. Lee, Ig Window Unit Having Triple Silver Coating and Dielectric Coating on Opposite Sides of Glass Substrate, WO2018165645A1, 2018.
[30] H. Cao, J. Zhang, B. Yang, F. Huang, K. Fukuhara, Three-silver Low-Emissivity Glass and Preparation Method Thereof, CN114409273A, 2022.
[31] R. Alcain, E. Carretero, R. Chueca, C. Heras, I. Salinas, Study of optical, thermal and radio frequency properties of low emissivity coatings with frequency selective surfaces, J. Phys. D Appl. Phys. 55 (2022), 065502, https://doi.org/10.1088/1361-6463/ac31f1.
[32] European Standard, European Committee for Standardization, EN 410, Glass in Building—Determination of Luminous and Solar Characteristics of Glazing, EN 410, European Standard, European Committee for Standardization, 2011.
[33] European Standard, European Committee for Standardization, EN 12898, Glass in Building—Determination of the Emissivity, European Standard, European Committee for Standardization, 2019.
[34] H.J. Glaser, Large Area Glass Coating, Von Ardenne Anlagentechnik, Dresden, 2000.
[35] J.C. Augusto de Queiroz, J.B. de Azevedo Filho, J.Q. de Medeiros Neto, I. O. Nascimento, I.A. de Souza, M.G. de Oliveira Queiroz, E.B. de Melo, J.D. Diniz Melo, T.H. de Carvalho Costa, Structural and optical properties of Al-doped ZnO thin films produced by magnetron sputtering, Process, Appl. Ceram. 14 (2020) 119–127, https://doi.org/10.2298/PAC2002119Q.
[36] J. Ray, M. Desai, C. Panchal, P. Patel, Magnetron sputtered Al-ZnO thin films for photovoltaic applications, J. Nano- Electron. Phys. 3 (2011) 755.
[37] Y. Xia, P. Wang, S. Shi, M. Zhang, G. He, J. Lv, Z. Sun, Deposition and characterization of AZO thin films on flexible glass substrates using DC magnetron sputtering technique, Ceram. Int. 43 (2017) 4536–4544, https://doi.org/10.1016/j.ceramint.2016.12.106.

[38] H.X. Chen, J.J. Ding, X.G. Zhao, S.Y. Ma, Microstructure and optical properties of ZnO:Al films prepared by radio frequency reactive magnetron sputtering, Physica B 405 (2010) 1339–1344, https://doi.org/10.1016/j.physb.2009.11.085.
[39] K. Seawsakul, M. Horprathum, P. Eiamchai, V. Pattantsetakul, S. Limwichean, P. Muthitamongkol, C. Thanachayanont, P. Songsiriritthigul, Effects of sputtering power toward the Al-doped ZnO thin Film prepared by pulsed DC magnetron sputtering, in: MATERIALS TODAY-PROCEEDINGS, Elsevier Science Bv, Amsterdam, 2017, pp. 6466–6471, https://doi.org/10.1016/j.matpr.2017.06.154.
[40] M. Shiravand, N. Ghobadi, E.G. Hatam, The investigation of structural, surface topography, and optical behaviors of Al-doped ZnO thin films with annealing temperature deposited by RF magnetron sputtering, J. Mater. Sci. Mater. Electron. 34 (2023) 713, https://doi.org/10.1007/s10854-023-10110-9.
[41] S.-M. Kim, Y.-S. Rim, M.-J. Keum, K.-H. Kim, Influence of a Ag layer on AZO/Ag/AZO multilayer thin films prepared by facing targets sputtering, J. Kor. Phys. Soc. 54 (2009) 1302–1308, https://doi.org/10.3938/jkps.54.1302.